Mechanics of Advanced Composite Structures 9 (2022) 11-23

Semnan University

Mechanics of Advanced Composite Structures

journal homepage: http://MACS.journals.semnan.ac.ir

A Novel Approach for Lateral Buckling Assessment of Double Tapered Thin-Walled Laminated Composite I-Beams

M. Soltani*

Department of Civil Engineering, Faculty of Engineering, University of Kashan, Kashan, Iran.

KEYWORDS

Lateral buckling
Laminated composites
Tapered I-beam
Classical lamination theory
Ritz method

ABSTRACT

The purpose of this paper is to introduce a simple and novel method for discussing the lateral-torsional stability of thin-walled symmetric balanced laminated beams with varying I-section. Based on the classic lamination theory and Vlasov's model, the total potential energy for the flexural displacements and the twist angle is established. The variational formulation is then constructed only in terms of the angle of twist using an auxiliary function. The buckling loads are finally determined by applying the Ritz method. To demonstrate the accuracy of the proposed formulation, the analytical solutions for a sample case of tapered I-beam are compared with results obtained from ANSYS's shell element. Moreover, this new procedure is very efficient in reducing the computational effort. Eventually, based on a selected load, the influences of some parameters such as the tapering ratios, transverse load position, and fiber orientation on lateral stability resistance of composite tapered I-beams under simply supported end conditions are discussed in detail. The results show that the lateral buckling resistance of composite beam with tapered I-section decreases significantly as the fiber angle in both flanges is rotated off-axis. Also, the maximum lateral buckling load for simply supported web and flanges tapered beam under uniformly distributed load is obtained by placing fibers$\pm 45^{\circ}$ in the web and 0° in both flanges.

1. Introduction

The use of thin-walled structural components in the most innovative engineering fields, including aircraft wings, helicopters, turbine blades, steel frames, and decks of the bridge, has become increasingly common throughout the years. Although thin-walled open cross-sections have some outstanding features, such as the high value of stiffness-to-weight and strength-to-weight ratios, they have some drawbacks, such as poor torsion rigidity and low out-of-plane bending resistance. As a result of these disadvantages, a laterally unbraced thin-walled beam subjected to bending around its strong axis may suddenly buckle in a flexural–torsional mode. This situation hence results in a lower stability strength. Moreover, in recent years, the application of thin-walled beams with variable cross-section has been extensively come into vogue in many advanced industries such as aeronautical and mechanical installations due to the importance of having an optimum distribution of weight and strength. With the development of fabrication processes, specifically pultrusion, thin-walled structural components made up of fiber-reinforced composite materials in aeronautical and mechanical installations have become increasingly common throughout the years. The main reason for this increase is the desirable feature of composites, such as high fatigue resistance, durability, corrosion resistance, and high stiffness-to-weight and strength-to-weight ratios. A review of the literature shows that different researchers have conducted several investigations to study the mechanical responses of thin-walled structural components made up of homogenous and/or composite materials. In the following, a short description of a few of them is presented.

Rajasekaran and Nalinaa [1] assessed the vibrational characteristics and buckling behavior of non-prismatic composite spatial members

* Corresponding author. Tel.: +983155912412; Fax: +983155912424
E-mail address: msoltani@kashanu.ac.ir

DOI: 10.22075/macs.2021.22105.1313
Received 2020-12-14; Received in revised form 2021-08-06; Accepted 2021-12-13.

with generic thin-walled sections via the finite element method within the context of non-linear strain displacement relationship. Based on a geometrically non-linear theory and the assumptions of large displacements and rotations, Machado and Cortinez [2-5] studied the free vibrational response and buckling behavior of composite beams with doubly-symmetric thin-walled open cross-section loaded by arbitrary external forces. Using the finite element methodology, the flexural-torsional coupled free vibrational behavior and buckling problem of thin-walled composite beams were precisely investigated by Vo and Lee [6], considering the impacts of axial load on the vibration characteristics. Based on linear fracture mechanics and the Castigliano theory, the influence of edge crack ratio and position on free vibration responses and lateral buckling strength of laminated composite slender beam was studied by Karaagac et al. [7]. To estimate the buckling resistance of simply supported thin-walled structural members made of Fiber Reinforced Polymer (FRP) loaded by axial and uniformly transverse forces, Ascione et al. [8] developed a mechanical model based on the assumptions of small strains and moderate rotations. In order to exhaustively examine the static and dynamic responses of beams made from FG piezoelectric materials, an innovative and improved three-noded beam element was formulated by Lezgy-Nazargah et al. [9]. Moreover, the elastic behavior of functionally graded piezomagnetic cylinders was studied in Refs. [10-13] under thermal, longitudinally non-uniform pressure, magnetic and mechanical loads. Using updated Lagrangian formulation, Lanc et al. [14] analyzed the lateral buckling and post-buckling behavior of functionally graded materials (FGMs), thin-walled beams with mono-symmetric I and channel sections for various boundary conditions based on Vlasov theory for thin-walled cross-sections and Euler–Bernoulli beam assumptions. Within the framework of finite stain theory, Mohandes and Ghasemi [15, 16] investigated nonlinear free vibrational characteristics of laminated beams through different shear deformation theories. Based on Ritz and Galerkin's methods, Saoula et al. [17] studied the stability resistance of laterally unrestrained simply supported thin-walled box beam elements subjected to combined bending and axial forces. Ghasemi and Mohandes [18-20] assessed the mechanical response including interlaminar normal and shear stresses of laminated composite size-dependent beam in the thermal and/or subjected to transverse load, according to finite strain assumption and a modified couple stress theory. To facilitate and increase the speed of mathematical computations to perform the elasto-plastic analysis of thin-walled beams, an innovative finite element formulation was suggested by Lezgy-Nazargah [21] based on the theory of generalized layered global-local beam (GLGB). Moreover, Nguyen et al. [22, 23] proposed a new finite element solution for computing lateral-torsional critical loads of FGM thin-walled beams with singly symmetric open sections. The precise free vibrational behavior of a doubly curved piezoelectric nanoshell resting on Pasternak's foundation was completely studied by Arefi [24] according to the first-order shear deformation theory. In another study, Ahmadi and Rasheed [25] employed the generalized semi-analytical technique to analyze the lateral-torsional buckling of anisotropic laminated beams with the rectangular thin-walled cross-section under simply supported end supports based on the classical laminated plate theory. Within the context of first-order shear deformation theory and using a semi-analytical solution methodology, the mechanical response of thin-walled laminated beams with constant open and/or closed cross-sections was assessed by Wackerfuß and Kroker [26]. In addition, Arefi and Zenkor [27] applied the higher-order sinusoidal shear deformation beam theory to extract the governing equations of sandwich microbeams with two piezoelectric face-layers and a homogeneous core loaded by a transverse force along with an electrical one. Using Navier's solution, Ghasemi and Meskini [28] assessed the free vibrational response of simply supported porous laminated rotating circular cylindrical shells within the framework of Love's shell theory. The lateral-torsional stability analysis of tapered thin-walled beam with arbitrary open cross-section under different boundary conditions was completely investigated by Soltani et al. [29-33] using different numerical methodologies. Ghasemi et al. [34-37] analyzed fiber-metal laminate (FML) cylindrical shells under different boundary conditions. For further numerical techniques-based investigations on the static and dynamic analyses, the reader is referred to [38-45] for composite beams subjected to different loading cases and end conditions.

Due to the application of composite structural members with thin-walled cross-sections in the design of sensitive and modern structures such as aircraft wings, helicopters, and turbine blades, it is necessary to study the problem of sandwich laminated thin-walled beams with varying cross-section. For this reason, the main aim of the present work is to analyze the lateral stability of laminated doubly-symmetric tapered I-beams with symmetrical lay-up for all section walls by presenting an innovative analytical solution.

Within the classic lamination theory framework and Vlasov's model without considering the shear deformation, the total potential energy for the vertical and lateral deformations and the twist angle are determined. Note that bending–twisting coupling is accounted for in our formulation. Based on the method proposed by Soltani et al. [31-33] and using an auxiliary function, the variational statement is then obtained only in terms of the twist angle. The acquired formulation can be applied for estimating the lateral-buckling load of composite I-beam under different boundary conditions. However, simply supported beam with free warping at both supports is contemplated here. The trigonometric function, which satisfies the simply supported beam end conditions, is thus used to acquire the analytical solutions through the Ritz method. The superiority of the proposed approach is to simplify and drastically decrease the essential computational efforts to calculate the lateral buckling load of symmetrically laminated thin-walled beams with varying cross-sections. To check the accuracy and the efficiency of the proposed methodology, our results are compared with numerical ones from the ANSYS code, and a good agreement is observed. For measuring the effects of web and flanges non-uniformity ratios, load height position, and fiber angle on lateral-torsional stability of simply supported laminated composite web and/or flanges tapered I-beams under uniformly distributed load, an exhaustive numerical example is finally presented.

2. Derivation of formulation

2.1. Geometrical description of double tapered I-beam

In the current study, the linear lateral-torsional buckling analysis is conducted for a laminated composite I-beam with a tapered web and flanges. The right-hand Cartesian coordinate system, with x as the initial longitudinal axis measured from the left end of the beam, the y-axis in the lateral direction, and the z-axis along the vertical direction, are considered as indicated in Fig. 1. The origin of these axes (O) is located at the centroid of the doubly-symmetric I-section. The symmetrically laminated I-beam is initially subjected to a laterally distributed load q_z in z-direction along with a line (PP'). The arbitrarily distributed force is thus applied on point P located on the section contour with the eccentricity $z_P(x)$ (Fig. 1).

In this study, Vlasov's model for non-uniform torsion is applied for the description of the displacement field of a point on the section contour. Based on this classical theory, only slender and long beams are considered and there are no shear deformations in the mean surface of the section. It is further admitted that the cross-section does not change shape during deflection. This means that the cross-section is rigid in its own plane and consequently no distortional deformations occur. From these assumptions, the displacement fields for an arbitrary point on the beam can be expressed as follows [46]:

$$\begin{aligned} U(x,y,z) &= u_0(x) - y\frac{dv(x)}{dx} \\ &\quad -z\frac{dw(x)}{dx} - \omega(y,z)\frac{d\theta(x)}{dx} \\ V(x,y,z) &= v(x) - z\theta(x) \\ W(x,y,z) &= w(x) + y\theta(x) \end{aligned} \tag{1}$$

In these equations, U is the axial displacement and displacement components V and W represent lateral and vertical displacements (in direction y and z). Note that the axial displacement U is extracted from the nullity of shear deformations in the main surface. The term $\omega(y,z)$ signifies a cross-section variable that is called the warping function, which can be defined based on Vlasov's torsion theory. u_0, v, and w are the 3D displacement components of the reference point O. θ is twisting angle.

2.2. Total potential energy for a composite beam with tapered I-section

The equilibrium equations for beam are derived from the potential energy condition given by:

$$\delta\Pi = \delta(U_l + U_0 - W_e) = 0 \tag{2}$$

δ illustrates a virtual variation in the last formulation. U_l represents the elastic strain energy, U_0 expresses the strain energy due to effects of the initial stresses and W_e is the work of the applied loads. According to the applied load, $\delta\Pi$ is reduced to the following terms:

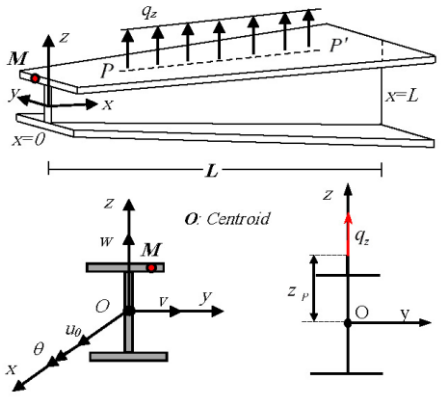

Fig. 1. Geometrical scheme for doubly symmetric I-section beam subjected to an arbitrarily distributed external load

$$\begin{aligned}\delta\Pi = &\int_0^L\int_A\left(\sigma_{xx}\delta\varepsilon_{xx}^{l}+\sigma_{xy}\delta\gamma_{xy}^{l}\right.\\ &\left.+\sigma_{xz}\delta\gamma_{xz}^{l}\right)dAdx\\ +&\int_0^L\int_A\left(\sigma_{xx}^{0}\delta\varepsilon_{xx}^{*}+\sigma_{xy}^{0}\delta\gamma_{xy}^{*}\right.\\ &\left.+\sigma_{xz}^{0}\delta\gamma_{xz}^{*}\right)dAdx\\ -&\int_0^L q_z\delta w_p dx=0\end{aligned} \tag{3}$$

in which, L and A express the beam length and the cross-sectional area, respectively. $(\delta\varepsilon_{xx}^{l},\delta\gamma_{xz}^{l},\delta\gamma_{xy}^{l})$ and $(\delta\varepsilon_{xx}^{*},\delta\gamma_{xz}^{*},\delta\gamma_{xy}^{*})$ are the variation of the linear and the non-linear parts of the strain tensor, respectively. σ_{ij}denotes the Piola–Kirchhoff stress tensor, and σ_{ij}^{0} is the initial stress, also called *the pre-buckling stress*. Based on the assumption of Green's strain-tensor, the linear and the non-linear parts of strain-displacement relations and their first variation are [29, 31]:

$$\begin{aligned}&\varepsilon_{xx}^{l}=u_0'-yv''-zw''-\omega\theta''\\ &\delta\varepsilon_{xx}^{l}=\delta u_0'-y\delta v''-z\delta w''-\omega\delta\theta''\\ &\varepsilon_{xx}^{*}=\frac{1}{2}(v'^2+w'^2+r^2\theta'^2)\\ &+yw'\theta'-zv'\theta'\\ &\delta\varepsilon_{xx}^{*}=v'\delta v'+w'\delta w'+r^2\theta'\delta\theta'\\ &\quad+y\theta'\delta w'+yw'\delta\theta'-z\theta'\delta v'-zv'\delta\theta'\\ &with\ r^2=y^2+z^2\\ &\gamma_{xz}^{l}=2\varepsilon_{xz}^{l}=\left(y-\frac{\partial\omega}{\partial z}\right)\theta'\\ &\delta\gamma_{xz}^{l}=\left(y-\frac{\partial\omega}{\partial z}\right)\delta\theta'\\ &\gamma_{xz}^{*}=-(v'+\theta' z)\theta\\ &\delta\gamma_{xz}^{l}=-\theta\delta v'-v'\delta\theta\\ &\quad-z\theta\delta\theta'-z\theta'\delta\theta\\ &\gamma_{xy}^{l}=2\varepsilon_{xy}^{l}=-\left(z+\frac{\partial\omega}{\partial y}\right)\theta'\\ &\delta\gamma_{xy}^{l}=-\left(z+\frac{\partial\omega}{\partial y}\right)\delta\theta'\\ &\gamma_{xy}^{*}=(w'+\theta' y)\theta\\ &\delta\gamma_{xy}^{*}=\theta\delta w'+w'\delta\theta+y\theta\delta\theta'+y\theta'\delta\theta\end{aligned} \tag{4}$$

In this study, the applied external loads in the z-direction cause the pre-buckling shear force (V_z^0) and the pre-buckling bending moment (M_y^0) loading. Both these forces induce the pre-buckling axial and shear stresses as

$$\begin{aligned}&\sigma_{xx}^{0}=-\frac{M_y^0}{I_y}z,\qquad \sigma_{xz}^{0}=\frac{V_z^0}{A}=-\frac{M_y^{0'}}{A},\\ &\sigma_{xy}^{0}=0\end{aligned} \tag{5}$$

where $\sigma_{xx}^{0}$and $(\sigma_{xz}^{0},\sigma_{xy}^{0})$ are the pre-buckling bending stress and shear stress often called *the initial stresses*. In Eq. (3), w_P is the vertical displacement of point *P*. According to kinematics used in Asgarian et al. [29] and by adopting the quadratic approximation, the vertical displacement of the point P and its first variation are as:

$$w_P=w-z_P\frac{\theta^2}{2}\rightarrow\ \delta w_P=\delta w-z_P\theta\delta\theta \tag{6}$$

In this equation, z_P is used to imply the eccentricity of the applied loads from the centroid of the cross-section. Substituting equations (4) to (6) into relation (3), the expression of the virtual potential energy can be carried out as:

$$\begin{aligned}\delta\Pi=&\int_0^L\int_A\sigma_{xx}\begin{pmatrix}\delta u_0'-y\delta v''-z\delta w''\\-\omega\delta\theta''\end{pmatrix}dAdx\\ &+\int_0^L\int_A\tau_{xy}\left(-(z+\frac{\partial\omega}{\partial y})\delta\theta'\right)dAdx\\ &+\int_0^L\int_A\tau_{xz}\left((y-\frac{\partial\omega}{\partial z})\delta\theta'\right)dAdx\\ &+\int_0^L\int_A(-\frac{M_y^0}{I_y}z)\begin{pmatrix}v'\delta v'+w'\delta w'\\+r^2\theta'\delta\theta'\\+y\theta'\delta w'+yw'\delta\theta'\\-z\theta'\delta v'-zv'\delta\theta'\end{pmatrix}dAdx\\ &+\int_0^L\int_A(-\frac{M_y^{0'}}{A})\begin{pmatrix}-\theta\delta v'-v'\delta\theta\\-z\theta\delta\theta'-z\theta'\delta\theta\end{pmatrix}dAdx\\ &-\int_0^L(q_z\delta w-M_t\theta\delta\theta)dx=0\end{aligned} \tag{7}$$

in which, $M_t=q_z z_P$ denotes the second order torsion moments due to load eccentricity. The variation of strain energy can be formulated in terms of section forces acting on cross-sectional contour of the elastic member in the buckled configuration. The section stress resultants are presented by the following expressions:

$$N=\int_A\sigma_{xx}dA \tag{8a}$$

$$M_y=\int_A\sigma_{xx}zdA \tag{8b}$$

$$M_z=-\int_A\sigma_{xx}ydA \tag{8c}$$

$$B_\omega=-\int_A\sigma_{xx}\omega dA \tag{8d}$$

$$M_{sv}=\int_A\left(\tau_{xz}\left(y-\frac{\partial\omega}{\partial z}\right)-\tau_{xy}(z+\frac{\partial\omega}{\partial y})\right)dA \tag{8e}$$

where N is the axial force applied at end member. M_y and M_z denote the bending moments about major and minor axes, respectively. B_ω is the bi-moment. M_{sv} is the St-Venant torsion moment. In this stage, by integrating Eq. (7) over the cross-section area of the beam and using relations (8a)–(8e), the final form of the variation of total potential energy ($\delta\Pi$) is acquired as:

$$\begin{aligned}\delta\Pi = &\int_L \begin{pmatrix} N\delta u_0' + M_z\delta v'' \\ -M_y\delta w'' + B_\omega\delta\theta'' \end{pmatrix} dx \\ &+ \int_0^L (M_{sv}\delta\theta')\,dx \\ &+ \int_0^L \left(M_y^0(\theta'\delta v' + v'\delta\theta')\right)dx \\ &+ \int_0^L \left(M_y^{0'}(\theta\delta v' + v'\delta\theta)\right)dx \\ &- \int_0^L (q_z\delta w - q_z z_P\theta\delta\theta)dx = 0\end{aligned} \tag{9}$$

or

$$\begin{aligned}&\delta\Pi = \\ &\int_L \begin{pmatrix} N\delta u_0' + M_z\delta v'' \\ -M_y\delta w'' + B_\omega\delta\theta'' + M_{sv}\delta\theta' \end{pmatrix} dx \\ &+ \int_0^L \left(-M_y^0 v''\delta\theta - M_y^0\theta\delta v''\right)dx \\ &- \int_0^L (q_z\delta w - q_z z_P\theta\delta\theta)dx = 0\end{aligned} \tag{10}$$

The present model is applied in the case of balanced and symmetrical lay-ups of the web and both flanges. In the context of classical laminated plate theory and substitution Eq. (4) into Eq. (8), the stress resultants of symmetrically balanced laminates are derived in terms of displacement components as [47]

$$N = (EA)_{com}u_0' \tag{11a}$$

$$M_z = (EI_z)_{com}v'' \tag{11b}$$

$$M_y = -(EI_y)_{com}w'' \tag{11c}$$

$$B_\omega = (EI_\omega)_{com}\theta'' \tag{11d}$$

$$M_{sv} = (GJ)_{com}\theta' \tag{11e}$$

where $(EA)_{com}$denotes axial rigidity. $(EI_y)_{com}$and $(EI_z)_{com}$ represent the flexural rigidities of the y- and z-axes, respectively. $(EI_\omega)_{com}$and $(GJ)_{com}$are, respectively, warping and torsional rigidities of composite thin-walled beams with doubly symmetric I-section, defined by [47]:

$$(EA)_{com} = 2bA_{11}^f + dA_{11}^w \tag{12a}$$

$$(EI_y)_{com} = 2bD_{11}^f + \frac{d^2}{2}bA_{11}^f + \frac{d^3}{12}A_{11}^w \tag{12b}$$

$$(EI_z)_{com} = \frac{b^3}{6}A_{11}^f + dD_{11}^w \tag{12c}$$

$$(EI_\omega)_{com} = \left(\frac{d^2}{4}A_{11}^f + D_{11}^f\right)\frac{b^3}{6} + \frac{d^3}{12}D_{11}^w \tag{12d}$$

$$(GJ)_{com} = 4(2bD_{66}^f + dD_{66}^w) \tag{12e}$$

That indexes f and w refer to the web and the flange of the beam cross-section, respectively. $A_{11}^f, A_{11}^w$and $D_{11}^f, D_{11}^w, D_{66}^f, D_{66}^w$ are the matrices of extensional and bending stiffness of both flanges and web, respectively, which are calculated as

$$\begin{aligned}(A_{ij}^f, D_{ij}^f) &= \int Q_{ij}^f(1, z^2)dz \\ (A_{ij}^w, D_{ij}^w) &= \int Q_{ij}^w(1, y^2)dy\end{aligned} \tag{13}$$

where $Q_{ij}^f$and $Q_{ij}^w$are the transformed reduced stiffness related to the flanges and web, respectively. Since the breadth of the flanges and the height of the web are assumed to vary linearly along the length of the beam, the above stiffness terms Eq. (12) are not constant.

Substituting Eq. (11) into (10), one gets the variation of the total potential is then a function of the virtual displacements $\delta u_0, \delta v, \delta w$and $\delta\theta$, and of their derivatives as

$$\begin{aligned}&\delta\Pi = \\ &\int_L \begin{pmatrix} (EA)_{com}u_0'\delta u_0' + (EI_z)_{com}v''\delta v'' \\ +(EI_y)_{com}w''\delta w'' \\ +(EI_\omega)_{com}\theta''\delta\theta'' + (GJ)_{com}\theta'\delta\theta' \end{pmatrix} dx \\ &+ \int_0^L \left(-M_y^0 v''\delta\theta - M_y^0\theta\delta v''\right)dx \\ &- \int_0^L (q_z\delta w - q_z z_P\theta\delta\theta)dx = 0\end{aligned} \tag{14}$$

or equivalently

$$\int_L \left((EA)_{com}u_0'\delta u_0'\right)dx = 0 \tag{15a}$$

$$\int_L \left((EI_y)_{com}w''\delta w'' - q_z\delta w\right)dx = 0 \tag{15b}$$

$$\int_L \left((EI_z)_{com}v'' - M_y^0\theta\right)\delta v''dx = 0 \tag{15c}$$

$$\int_L \begin{pmatrix} (EI_\omega)_{com}\theta''\delta\theta'' + (GJ)_{com}\theta'\delta\theta' \\ -M_y^0 v''\delta\theta - z_P q_z\theta\delta\theta \end{pmatrix} dx = 0 \tag{15d}$$

Based on the straightforward methodology presented by Soltani et al. [29-33], Eq. (15c) can be rewritten in the following form for any acceptable lateral buckled configuration:

$$v'' = \frac{M_y^0}{(EI_z)_{com}}\theta \tag{16}$$

whose substitution in Eq. (15d) enables its redefinition in an uncoupled form just dependent on the twist angle θ, independently from the lateral displacement v, i.e.

$$\int_L \begin{pmatrix} (EI_\omega)_{com}\theta''\delta\theta'' + (GJ)_{com}\theta'\delta\theta' \\ -\frac{M_y^{0\,2}}{(EI_z)_{com}}\theta\delta\theta - z_P q_z \theta\delta\theta \end{pmatrix} dx = 0 \quad (17)$$

One of the most convenient methodologies to precisely estimate the lateral-torsional stability limit state of different types of continuous structural elements is the Rayleigh-Ritz method. Additionally, the main advantage of the present approach is that the Central Processing Unit (CPU) requires less time to acquire the solution with excellent precision [30, 31]. In the following, the Rayleigh-Ritz method is thus employed to obtain buckling load of non-prismatic columns. Based on the assumptions of this classical technique, it is essential to replace buckled shape of the elastic beam with appropriate deformation shapes of the element after lateral buckling satisfying both geometrical and natural boundary conditions of the system. Since the resulting weak form of lateral equilibrium equations is only in terms of the twisting angle, the approximate buckled shape of the beam must satisfy all the essential boundary conditions for torsional rotation.

In the case of cantilevers, the left end (fixed one) of the beam is prevented from freely warping ($\theta(0) = \theta'(0) = 0$), while, the right end of the I-section is free to warp ($\theta''(L) = 0$). Thus, the first displacement mode in torsion can be approximated by trigonometric functions as [48, 49]

$$\begin{aligned} \theta(x) &= \theta_1\left(1 - cos\left(\frac{\pi x}{2L}\right)\right) \\ &+\theta_2\left(1 - cos\left(\frac{3\pi x}{2L}\right)\right) \\ &+\theta_3(1 - cos\left(\frac{5\pi x}{2L}\right)) \end{aligned} \quad (18)$$

For simply supported beams, the twist angle equals zero at both ends ($\theta(0) = \theta(L) = 0$). Further, the ends of the I-shape beam are free to warp ($\theta''(0) = \theta''(L) = 0$). Therefore, the torsional rotation mode shape becomes [48, 49]:

$$\theta(x) = \theta_1\, sin\left(\frac{\pi x}{L}\right) \quad (19)$$

For fixed-fixed cases, both end supports are prevented from freely warping. This means that the twist angle and the rate of twist at the fixed support are null ($\theta(0) = \theta(L) = \theta'(0) = \theta'(L) = 0$). The expression for the angle of twist can be approximated as [48, 49]

$$\begin{aligned} \theta(x) &= \theta_1(1 - cos\left(\frac{2\pi x}{L}\right)) \\ &+\theta_2(1 - cos\left(\frac{3\pi x}{L}\right)) \\ &+\theta_3(1 - cos\left(\frac{5\pi x}{L}\right)) \end{aligned} \quad (20)$$

In the above equations, $\theta_i (i = 1,2,3)$ are the Ritz coefficients. It is important to note that the final variational formulation (Eq. (17)) is applicable for lateral stability analysis of composited tapered I-beam under various end conditions [29, 30, 33, 48], but, in the next section, only simply supported beam is considered for implementation of the Ritz method.

2.3. Lateral buckling analysis

To demonstrate the application of Eq. (17), simply supported beam subjected to uniformly distributed load is considered, as shown in Fig. 2. For this loading condition, the bending moment distribution through the x-axis is given by:

$$M_y^0 = q_z \frac{L^2}{2}\left(\frac{x}{L} - \frac{x^2}{L^2}\right) \quad (21)$$

The substitution of the expression of the internal bending moment, the corresponding buckled shape function of the simply supported beam Eq. (19), and its derivatives into Eq. (17) yields.

$$\begin{aligned} &\int_L \left(\left(\frac{1}{4} q_z{}^2 \frac{(Lx - x^2)^2}{(EI_z)_{com}} + z_P q_z\right)(sin\left(\frac{\pi x}{L}\right))^2 \right) dx \\ &= \left(\frac{\pi}{L}\right)^2 \int_L \begin{pmatrix} \left(\frac{\pi}{L}\right)^2 (EI_\omega)_{com}(sin\left(\frac{\pi x}{L}\right))^2 \\ +(GJ)_{com}(cos\left(\frac{\pi x}{L}\right))^2 \end{pmatrix} dx \end{aligned} \quad (22)$$

Again remind that in the present study, the height of the web and the width of both flanges are varying linearly such as

$$\begin{aligned} d(x) &= d_0(1 + \alpha)\left(\frac{x}{L}\right) + d_0 \\ b(x) &= b_0(1 + \beta)\left(\frac{x}{L}\right) + b_0 \end{aligned} \qquad 0 \le \alpha, \beta \quad (23)$$

The terms$\beta$and$\alpha$are the flanges and web tapering ratios, respectively, which are defined as $\beta = b_L/b_0 - 1$ and $\alpha = d_L/d_0 - 1$. The subscripts 0 and L indicate dimensions at *x=0* and x=L. Note that the prismatic cross-sections case is achieved by equating these two parameters (βandα) to zero.

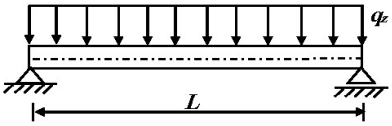

Fig. 2. Simply supported beam with uniformly distributed load.

The three stiffness quantities required for lateral-torsional stability of double tapered I-beam subjected to transverse loading are finally determined by substitution Eq. (23) into Eq. (12).

$$(EI_z)_{com} = \frac{1}{6}\left(b_L(1+\beta)\left(\frac{x}{L}\right)+b_L\right)A_{11}^f + \left(d_L(1+\alpha)(\frac{x}{L})+d_L\right)D_{11}^w \quad (24a)$$

$$(EI_\omega)_{com} = \frac{1}{6}\left(b_L(1+\beta)\left(\frac{x}{L}\right)+b_L\right)^3 D_{11}^f + \frac{1}{24}\left(d_L(1+\alpha)\left(\frac{x}{L}\right)+d_L\right)^2 \times \left(b_L(1+\beta)\left(\frac{x}{L}\right)+b_L\right)^3 A_{11}^f + \frac{1}{12}\left(d_L(1+\alpha)(\frac{x}{L})+d_L\right)^3 D_{11}^w \quad (24b)$$

$$(GJ)_{com} = 8\left(b_L(1+\beta)\left(\frac{x}{L}\right)+b_L\right)D_{66}^f + 4\left(d_L(1+\alpha)(\frac{x}{L})+d_L\right)D_{66}^w \quad (24c)$$

In this study, it is supposed that uniformly transverse load can be applied at three different positions: the top flange, the centroid (shear center), and the bottom flange and, therefore

$$z_P(x) = z_{P0}(1+\alpha)(\frac{x}{L}) + z_{P0}$$
$$z_{P0} = -\frac{d_0}{2}, 0, \frac{d_0}{2} \quad (25)$$

By inserting the equation presented above Eq.s (24 and 25) into Eq. (22) and after appropriate integrations over the beam's length, as well as some calculations, the critical values of q_z can be obtained.

3. Numerical Example

In the preceding section, an analytical methodology has been formulated to calculate the lateral-torsional buckling loads of thin-walled laminated composite beam with varying I-section. In this section, a comprehensive example is conducted to show the effects of significant parameters such as fiber angle orientation, loading position, and non-uniformity ratios (β, α) on the lateral buckling capacity of multi-layered composite tapered I-beam. To that end, a simply supported laminated double-tapered I-beam with symmetric lamination with a span of 8m subjected to uniformly distributed load is considered. At the left end section, both flanges are assumed to be 100mm wide (b_L), and the web of the I-shape is 200mm deep (d_L). All section walls (flanges and web) are assumed to be laminated symmetrically concerning its mid-plane and made of 16 plies, each 0.25mm thick (total thickness: t_w=t_f=4 mm). All the layers are made of glass/epoxy (S2) with the following elastic properties [2-5]:

$$E_1 = 48.3(GPa), \quad E_2 = 19.8(GPa),$$
$$G_{12} = 8.96(GPa), \quad G_{13} = 8.96(GPa),$$
$$G_{23} = 6.19(GPa), \quad \nu_{12} = 0.27,$$
$$\nu_{13} = 0.27, \quad \nu_{23} = 0.6.$$

where directions parallel and perpendicular to fibers are presented by subscripts '1' and '2', respectively. The main features of this type of glass epoxy composite are its high tensile strength, high resistance to damage, and improved impact resistance. Therefore, S-glass is widely used in the aerospace and building industries.

To have a better understanding of the numerical outcomes, the evaluated lateral-torsional buckling load is presented in the non-dimensional form as

$$q_{nor} = \frac{q_{cr}L^3}{E_y t_w d_L^3} \quad (26)$$

The current section is divided into two different subsections: the first one for verification of the formulation proposed herein, and the second one is for studying the influence of the above-mentioned factors on the linear lateral buckling behavior of the considered member.

3.1. Verification

The absence of numerical studies on the thin-walled laminated composite beams with varying cross-sections, herein, and the accuracy of the predicted results based on the present formulation are checked with those acquired via SHELL281 of ANSYS code [50]. To this end, the lowest values of the non-dimensional lateral buckling parameter (q_{nor}) of the contemplated beam with variable thin-walled I-section for two different loading positions and various values of tapering ratios ($\beta = \alpha = 0$, 0.2, and 0.5) are evaluated and depicted in Table 1. In this section, six different stacking sequences are considered for the web and flanges. Fig. 3 schematically shows two different lay-up arrangements of both flanges of the I-section. Additionally, the relative errors (Δ) associated with the current approach are given by the following expression:

$$\Delta = \frac{\left|q_{nor}^{Ritz} - q_{nor}^{ANSYS}\right|}{q_{nor}^{ANSYS}} \times 100 \quad (27)$$

One observes a good agreement between the present analytical methodology and ANSYS simulations. The error between the Ritz method and ANSYS is below 10%.

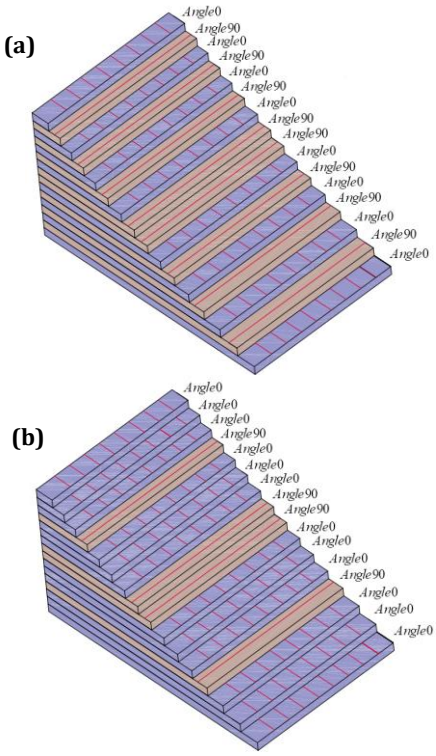

Fig. 3: Ply stack of top and bottom flanges, (a) $[0/90]_{4s}$, (b) $[(0_3/90)_2]_s$.

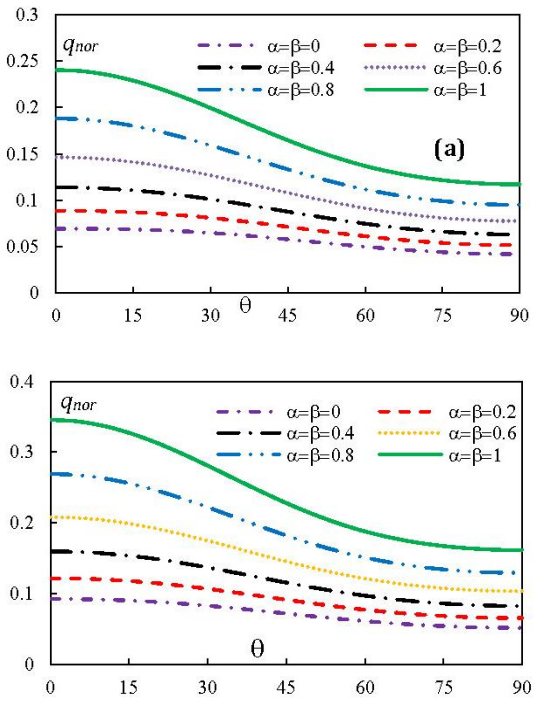

Fig. 4. Variation of the lateral buckling parameter with respect to fiber angle change in both flanges for different tapering ratios, (a) load applied at the top flange, (b) load applied at the centroid.

Table 1. Comparative evaluation of the lateral buckling response for a simply supported composite web and flanges tapered beam under distributed load.

Tapering parameter	Lay-up		Loading position					
			Top flange			Centroid		
	Flanges	web	Present	ANSYS	Δ(%)	Present	ANSYS	Δ(%)
$\beta_f = \beta_w = 0$	$[0]_{16}$	$[0]_{16}$	0.069	0.068	2.361	0.093	0.090	2.623
	$[0/90]_{4s}$	$[\pm45]_8$	0.064	0.060	5.742	0.081	0.077	5.223
	$[(0_3/90)_2]_s$	$[\pm45]_8$	0.071	0.067	5.675	0.091	0.087	5.163
	$[0/90]_{4s}$	$[0/90]_{4s}$	0.056	0.055	1.974	0.073	0.071	2.186
	$[0/90]_{4s}$	$[(0/\pm45/90)_2]_s$	0.060	0.058	2.939	0.077	0.075	2.953
	$[(0_3/90)_2]_s$	$[(0/\pm45/90)_2]_s$	0.067	0.065	2.990	0.087	0.084	3.015
$\beta_f = \beta_w = 0.2$	$[0]_{16}$	$[0]_{16}$	0.089	0.086	3.610	0.122	0.117	4.478
	$[0/90]_{4s}$	$[\pm45]_8$	0.079	0.074	6.413	0.103	0.097	6.548
	$[(0_3/90)_2]_s$	$[\pm45]_8$	0.089	0.083	6.373	0.118	0.110	6.520
	$[0/90]_{4s}$	$[0/90]_{4s}$	0.071	0.069	3.058	0.095	0.091	3.886
	$[0/90]_{4s}$	$[(0/\pm45/90)_2]_s$	0.075	0.072	3.889	0.099	0.095	4.539
	$[(0_3/90)_2]_s$	$[(0/\pm45/90)_2]_s$	0.084	0.081	3.994	0.113	0.108	4.654
$\beta_f = \beta_w = 0.5$	$[0]_{16}$	$[0]_{16}$	0.129	0.120	8.153	0.183	0.168	8.904
	$[0/90]_{4s}$	$[\pm45]_8$	0.110	0.100	9.301	0.148	0.135	9.569
	$[(0_3/90)_2]_s$	$[\pm45]_8$	0.125	0.114	9.594	0.171	0.156	9.829
	$[0/90]_{4s}$	$[0/90]_{4s}$	0.100	0.094	6.844	0.138	0.128	7.684
	$[0/90]_{4s}$	$[(0/\pm45/90)_2]_s$	0.105	0.098	7.323	0.143	0.132	8.047
	$[(0_3/90)_2]_s$	$[(0/\pm45/90)_2]_s$	0.120	0.111	7.788	0.166	0.153	8.454

3.2. Parametric Study

In this section, to assess the effect of fiber angle orientation, load height parameter, and web and flanges non-uniformity ratios, three cases are considered. It is necessary to note that the laminated non-uniform I-beam with equal web height and flanges width tapering ratios ($\beta = \alpha$) under a uniform loading distribution applied on the top flange and the shear center is studied.

The first case is that the web and flanges plates are made of 16 plies with unidirectional $[0]_{16}$lay-up for the web, while the top and bottom flanges are assumed to have symmetrical $[\pm\theta]_{4S}$lay-ups. In this case, Fig. 4 exhibits the effect of the non-uniformity ratio ($\beta = \alpha$) on the variation of the lateral buckling load parameters of laminated composite tapered I-beam considering the fiber angle (θ) of its flanges. It is seen that the lateral stability capacity decreases monotonically with an increase in fiber angle (θ), where the effect of fiber angle change increases when θ varies between 20 and 60. In the first lateral buckling mode, the laminated thin-walled beam becomes weaker and more unstable as the angle of orientation increases. The maximum lateral stability strength is thus obtained with unidirectional $[0]_{16}$lay-up for both flanges. In the case of a prismatic member, these results are confirmed in [47].

The next section is the same as before, except that the top and bottom flanges are considered unidirectional, $[0]_{16}$whereas the web laminate is assumed to have symmetric angle-ply laminations $[\pm\theta]_{4S}$. Now, to study the influence of fiber angle orientation in the web of doubly-symmetric I-section, the variation of lateral buckling parameters for a simply supported laminated tapered beam with various tapering ratios versus fiber angle change is presented in Fig. 5. As the fiber angle is rotated off axis, the lateral buckling capacity is maximized at θ = 45° and then sharply minimized at θ = 90°. The higher lateral stability strength for prismatic and tapered I-beam is thus obtained by aligning the fiber orientation in the web around 45°. Similar behavior can also be observed for the two different loading positions.

The third case is that all section walls, including flanges and the web, are sixteen-layered symmetric angle-ply laminate $[\pm\theta]_{4S}$with equal thickness. For this lay-up, Fig. 6 displays the variation of the lowest lateral buckling parameter of simply supported composite I-beam considering the change in fiber orientation in the flanges and web for six different tapering parameters ($\beta = \alpha$ = 0, 0.2, 0.4, 0.6, 0.8, and 1). Fig. 5 shows that the lateral stability decreased steadily with increasing fiber angle. In addition, as shown in Fig. 6, the magnitude of critical parameters relating to the first lateral buckling mode decreases sharply for $20 \leq \theta \leq 60$ whereas, the lateral buckling resistance decreases slightly and reaches the minimum magnitude for$\theta > 60$. Similar trends in the results are also observed.

According to the illustrations, it is found out that for any value of fiber angle orientation, the stability of prismatic beam ($\beta = \alpha = 0$) and double tapered one with $\beta = \alpha = 1$ is the minimum and maximum, respectively. Hence, the lateral buckling parameter increases significantly with an increase in web and/or flange non-uniformity ratios (β and α) due to the enhancement of all geometrical characteristics of cross-section and, consequently, flexural stiffness and torsional rigidity of the elastic member.

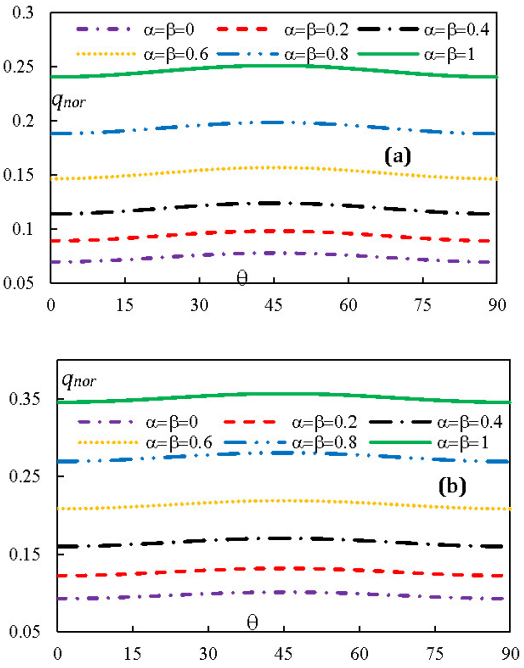

Fig. 5. Variation of the lateral buckling parameter with respect to fiber angle change in the web for different tapering ratios, (a) load applied at the top flange, (b) load applied at the centroid.

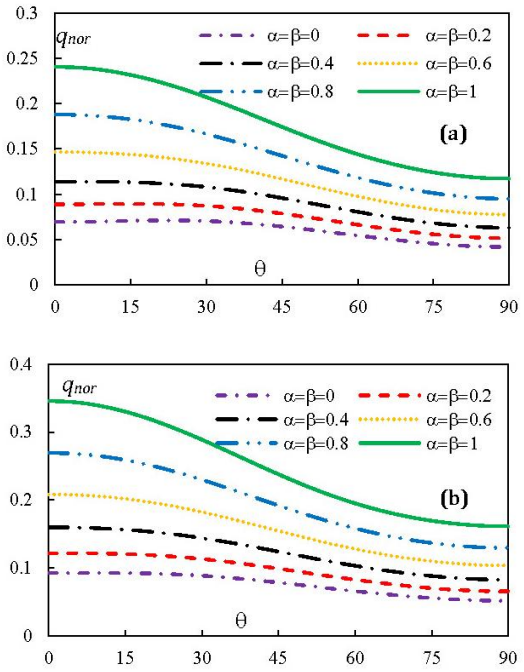

Fig. 6. Variation of the lateral buckling parameter with respect to fiber angle change in the web and both flanges for different tapering ratios, (a) load applied at the top flange, (b) load applied at the centroid.

Based on the results presented in Figs. 4-6, it can be concluded that the optimum fiber angles for achieving the highest lateral buckling resistance of simply supported web and flanges tapered beam under distributed load are $\pm 45^{\circ}$ in the web and 0°in both flanges. This statement is reasonable since the flexural stiffness $(EI_z)_{com}$and the warping rigidity$(EI_\omega)_{com}$, which are expressed in terms of unidirectional stiffness A_{11} and D_{11} (Eq. (24)), achieved their maximum magnitude by aligning the fibers at 0° in both flanges and web. As these two stiffness quantities ($(EI_z)_{com}$ and $(EI_\omega)_{com}$) are mostly controlled by the fiber angle on the top and bottom flanges, hence the fiber orientation should be placed at 0°in both flanges to improve the lateral stability strength. Based on Eq. (24), the laminate torsional stiffness $(GJ)_{com}$is presented in terms of twisting stiffness in both flanges D_{66}^{f} and the webD_{66}^{w}, which are often maximum for fiber orientation around45°. Therefore, the linear lateral-torsional capacity becomes higher by placing the web fiber angle at $\pm 45^{\circ}$.

In the following sections, the optimal stacking sequence is adopted. In order to investigate the influence of high load parameter (z_P) on the lateral stability behavior, the variations of the lateral buckling load parameters (q_{nor}) of the thin-walled laminated beam with varying I-section versus tapering ratios (varying from 0 to 1) is plotted in Fig. 7 for the three loading positions.

The magnitude of the non-dimensional lateral-torsional buckling parameter (q_{nor}) for various combinations of web height and flange width tapering ratios, with different loading positions are listed in Table 2.

Fig. 6 and Table 2 show that the uniformly transverse load position has a significant effect on the stability strength of composite beams with varying doubly-symmetric I-section, especially for larger tapering ratios. Regarding these load cases, the lateral buckling strength will become best when the distributed load location is on the bottom flange due to the reduction of the rotation of the I-section from its origin, and the lower values are obtained when the load is applied on the top flange position.

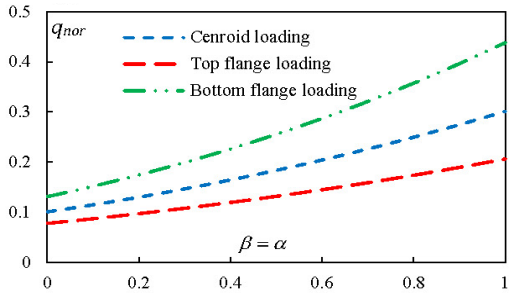

Fig. 7. Variation of the lateral buckling parameter versus the non-uniformity ratio for three different transverse loading positions

Table 2: Lateral buckling parameter for laminated tapered I-beam with different tapering ratios and loading position (top and bottom flanges: $[0]_{16}$, web: $[\pm 45]_{4s}$)

Loading position	β	Web tapering ratio (α)			
		0	0.3	0.6	0.9
Top flange	0	0.078	0.083	0.088	0.093
	0.3	0.102	0.110	0.118	0.127
	0.6	0.132	0.144	0.157	0.170
	0.9	0.168	0.186	0.204	0.223
Centroid	0	0.101	0.109	0.118	0.127
	0.3	0.137	0.150	0.163	0.176
	0.6	0.181	0.200	0.219	0.239
	0.9	0.233	0.260	0.288	0.317
Bottom flange	0	0.131	0.144	0.157	0.169
	0.3	0.182	0.199	0.217	0.234
	0.6	0.241	0.264	0.287	0.310
	0.9	0.308	0.338	0.368	0.397

Moreover, the effect of the rate of flanges width tapering parameter (β) is seen to be higher than the effect of the web non-uniformity ratio (α). The reason is that the lateral-torsional buckling phenomenon occurs concerning the minor axis moment of inertia.

4. Conclusions

In this paper, the lateral stability of a tapered thin-walled balanced laminated beam with an I-section is investigated by presenting an innovative analytical technique. It is assumed that all section walls (the web and both flanges) are laminated symmetrically concerning its mid-plane. Considering the bending–twisting coupling, the total potential energy is determined based on the assumptions of Vlasov's model and the classic lamentation theory. The resulting formulation is thus obtained in terms of the vertical and lateral deformations and the twist angle. By presenting an auxiliary function, the variational statement is established only in terms of the twist angle. The Ritz method is finally employed to estimate the lateral buckling load. It is believed that the methodology proposed herein facilitates lateral stability analysis of symmetrically laminated thin-walled beams with varying cross-sections. Therefore, this new procedure is very efficient in reducing computational effort and also saving computing time. After verification, the impact of web and/or flanges tapering ratios, fiber angle, and transverse loading position on lateral-torsional stability of simply supported composite tapered I-beam is exhaustively surveyed. According to the numerical outcomes, it is concluded that the mentioned parameters play significant roles in the stability strength of laminated tapered I-beam. For all transverse loading positions, it was found that the lateral buckling parameter of composite beam with tapered I-section decreases

as the fiber orientation in both flanges is rotated off axis, whereas the lateral-torsional buckling resistance increases as the web and/or flanges tapering ratios increase. It is also illustrated that the effect of the flange tapering parameter (β) on the buckling capacity is higher than that of the web one (α).

Additionally, it is observed that the buckling capacity of a simply supported laminated beam with doubly-symmetric I-section will become best when the uniformly distributed load is applied on the bottom flange. Also, it can be interpreted that the effect of fiber angle change in both flanges on lateral buckling strength is significant. Finally, it can be concluded that the maximum lateral buckling load for simply supported web and flanges tapered beam under uniformly distributed load is obtained by placing fibers at $\pm 45^{\circ}$ in the web and 0°in both flanges.

References

[1] Rajasekaran, S. and Nalinaa, K., 2005. Stability and vibration analysis of non-prismatic thin-walled composite spatial members of generic section. *International Journal of Structural Stability and Dynamics*, *5*(04), pp.489-520.

[2] Machado, S.P. and Cortínez, V.H., 2005. Non-linear model for stability of thin-walled composite beams with shear deformation. *Thin-Walled Structures*, *43*(10), pp.1615-1645.

[3] Machado, S.P. and Cortínez, V.H., 2007. Free vibration of thin-walled composite beams with static initial stresses and deformations. *Engineering Structures*, *29*(3), pp.372-382.

[4] Machado, S.P., 2007. Geometrically non-linear approximations on stability and free vibration of composite beams. *Engineering structures*, *29*(12), pp.3567-3578.

[5] Machado, S.P., 2008. Non-linear buckling and postbuckling behavior of thin-walled beams considering shear deformation. *International Journal of Non-Linear Mechanics*, *43*(5), pp.345-365.

[6] Vo, T.P. and Lee, J., 2009. Flexural–torsional coupled vibration and buckling of thin-walled open section composite beams using shear-deformable beam theory. *International Journal of Mechanical Sciences*, *51*(9-10), pp.631-641.

[7] Karaagac, C., Ozturk, H. and Sabuncu, M., 2013. Effects of an edge crack on the free vibration and lateral buckling of a cantilever laminated composite slender beam. *Journal of Vibration and Control*, *19*(16), pp.2506-2522.

[8] Ascione, L., Berardi, V.P., Giordano, A. and Spadea, S., 2013. Local buckling behavior of FRP thin-walled beams: a mechanical model. *Composite Structures*, *98*, pp.111-120.

[9] Lezgy-Nazargah, M., Vidal, P. and Polit, O., 2013. An efficient finite element model for static and dynamic analyses of functionally graded piezoelectric beams. *Composite Structures*, *104*, pp.71-84.

[10] Arefi, M., Rahimi, G.H. and Khoshgoftar, M.J., 2011. Optimized design of a cylinder under mechanical, magnetic and thermal loads as a sensor or actuator using a functionally graded piezomagnetic material. *International Journal of Physical Sciences*, *6*(27), pp.6315-6322.

[11] Arefi, M., Viertl, R. and Taheri, S.M., 2012. Fuzzy density estimation. *Metrika*, *75*(1), pp.5-22.

[12] Khoshgoftar, M.J., Rahimi, G.H. and Arefi, M., 2013. Exact solution of functionally graded thick cylinder with finite length under longitudinally non-uniform pressure. *Mechanics Research Communications*, *51*, pp.61-66.

[13] Arefi, M., Karroubi, R. and Irani-Rahaghi, M., 2016. Free vibration analysis of functionally graded laminated sandwich cylindrical shells integrated with piezoelectric layer. *Applied Mathematics and Mechanics*, *37*(7), pp.821-834.

[14] Lanc, D., Vo, T.P., Turkalj, G. and Lee, J., 2015. Buckling analysis of thin-walled functionally graded sandwich box beams. *Thin-Walled Structures*, *86*, pp.148-156.

[15] Mohandes, M. and Ghasemi, A.R., 2016. Finite strain analysis of nonlinear vibrations of symmetric laminated composite Timoshenko beams using generalized differential quadrature method. *Journal of Vibration and Control*, *22*(4), pp.940-954.

[16] Ghasemi, A.R. and Mohandes, M., 2017. Nonlinear free vibration of laminated composite Euler-Bernoulli beams based on finite strain using generalized differential quadrature method. *Mechanics of Advanced Materials and Structures*, *24*(11), pp.917-923.

[17] Saoula, A., Meftah, S.A. and Mohri, F., 2016. Lateral buckling of box beam elements under combined axial and bending loads. *Journal of Constructional Steel Research*, *116*, pp.141-155.

[18] Ghasemi, A.R. and Mohandes, M., 2016. Size-dependent bending of geometrically nonlinear of micro-laminated composite beam based on modified couple stress theory. *Mechanics of Advanced Composite Structures*, *3*(1), pp.53-62.

[19] Mohandes, M. and Ghasemi, A.R., 2017. Modified couple stress theory and finite strain assumption for nonlinear free

vibration and bending of micro/ nanolaminated composite Euler–Bernoulli beam under thermal loading. *Proceedings of the Institution of Mechanical Engineers, Part C: Journal of Mechanical Engineering Science*, *231*(21), pp.4044-4056.

[20] Ghasemi, A.R. and Mohandes, M., 2019. A new approach for determination of interlaminar normal/shear stresses in micro and nano laminated composite beams. Advances in Structural Engineering, 22(10), pp.2334-2344.

[21] Lezgy-Nazargah, M., 2017. A generalized layered global-local beam theory for elasto-plastic analysis of thin-walled members. *Thin-Walled Structures*, *115*, pp.48-57.

[22] Nguyen, T.T., Thang, P.T. and Lee, J., 2017. Flexural-torsional stability of thin-walled functionally graded open-section beams. *Thin-Walled Structures*, *110*, pp.88-96.

[23] Nguyen, T.T., Thang, P.T. and Lee, J., 2017. Lateral buckling analysis of thin-walled functionally graded open-section beams. *Composite Structures*, *160*, pp.952-963.

[24] Arefi, M., 2018. Nonlocal free vibration analysis of a doubly curved piezoelectric nano shell. *Steel and Composite Structures*, *27*(4), pp.479-493.

[25] Ahmadi, H. and Rasheed, H.A., 2018. Lateral torsional buckling of anisotropic laminated thin-walled simply supported beams subjected to mid-span concentrated load. *Composite Structures*, *185*, pp.348-361.

[26] Wackerfuß, J. and Kroker, A.M., 2018. An efficient semi-analytical simulation framework to analyse laminated prismatic thin-walled beams. *Computers & Structures*, *208*, pp.32-50.

[27] Arefi, M. and Zenkour, A.M., 2018. Size-dependent electro-elastic analysis of a sandwich microbeam based on higher-order sinusoidal shear deformation theory and strain gradient theory. *Journal of Intelligent Material Systems and Structures*, *29*(7), pp.1394-1406.

[28] Ghasemi, A.R. and Meskini, M., 2019. Free vibration analysis of porous laminated rotating circular cylindrical shells. *Journal of Vibration and Control*, *25*(18), pp.2494-2508.

[29] Asgarian, B., Soltani, M. and Mohri, F., 2013. Lateral-torsional buckling of tapered thin-walled beams with arbitrary cross-sections. *Thin-walled structures*, *62*, pp.96-108.

[30] Soltani, M., Asil Gharebaghi, S. and Mohri, F., 2018. Lateral stability analysis of steel tapered thin-walled beams under various boundary conditions. *Journal of Numerical Methods in Civil Engineering*, *3*(1), pp.13-25.

[31] Soltani, M., Asgarian, B. and Mohri, F., 2019. Improved finite element model for lateral stability analysis of axially functionally graded nonprismatic I-beams. *International Journal of Structural Stability and Dynamics*, *19*(09), p.1950108.

[32] Soltani, M. and Asgarian, B., 2020. Lateral-Torsional Stability Analysis of a Simply Supported Axially Functionally Graded Beam with a Tapered I-Section. *Mechanics of Composite Materials*, pp.1-16.

[33] Soltani, M. and Asgarian, B., 2021. Exact stiffness matrices for lateral–torsional buckling of doubly symmetric tapered beams with axially varying material properties. *Iranian Journal of Science and Technology, Transactions of Civil Engineering*, *45*(2), pp.589-609.

[34] Mohandes, M., Ghasemi, A.R., Irani-Rahagi, M., Torabi, K. and Taheri-Behrooz, F., 2018. Development of beam modal function for free vibration analysis of FML circular cylindrical shells. *Journal of Vibration and Control*, *24*(14), pp.3026-3035.

[35] Ghasemi, A.R. and Mohandes, M., 2019. Comparison between the frequencies of FML and composite cylindrical shells using beam modal function model. *Journal of Computational Applied Mechanics*, *50*(2), pp.239-245.

[36] Ghasemi, A.R. and Mohandes, M., 2020. Free vibration analysis of micro and nano fiber-metal laminates circular cylindrical shells based on modified couple stress theory. *Mechanics of Advanced Materials and Structures*, *27*(1), pp.43-54.

[37] Ghasemi, A.R., Kiani, S. and Tabatabaeian, A., 2020. Buckling analysis of FML cylindrical shells under combined axial and torsional loading. *Mechanics of Advanced Composite Structures*.

[38] Lezgy-Nazargah, M., 2014. An isogeometric approach for the analysis of composite steel–concrete beams. *Thin-Walled Structures*, *84*, pp.406-415.

[39] Lezgy-Nazargah, M. and Kafi, L., 2015. Analysis of composite steel-concrete beams using a refined high-order beam theory. *Steel and Composite Structures*, *18*(6), pp.1353-1368.

[40] Lezgy-Nazargah, M., Vidal, P. and Polit, O., 2019. A sinus shear deformation model for static analysis of composite steel-concrete beams and twin-girder decks including shear lag and interfacial slip effects. *Thin-Walled Structures*, *134*, pp.61-70.

[41] Lezgy-Nazargah, M., Vidal, P. and Polit, O., 2020. A penalty-based multifiber finite

element model for coupled bending and torsional-warping analysis of composite beams. *European Journal of Mechanics-A/Solids*, *80*, p.103915.

[42] Lezgy-Nazargah, M., 2020. A finite element model for static analysis of curved thin-walled beams based on the concept of equivalent layered composite cross section. *Mechanics of Advanced Materials and Structures*, pp.1-14.

[43] Lezgy-Nazargah, M., Vidal, P. and Polit, O., 2021. A quasi-3D finite element model for the analysis of thin-walled beams under axial–flexural–torsional loads. *Thin-Walled Structures*, *164*, p.107811.

[44] Einafshar, N., Lezgy-Nazargah, M. and Beheshti-Aval, S.B., 2021. Buckling, post-buckling and geometrically nonlinear analysis of thin-walled beams using a hypothetical layered composite cross-sectional model. *Acta Mechanica*, pp.1-18.

[45] Ghasemi, A.R., Heidari-Rarani, M., Heidari-Sheibani, B. and Tabatabaeian, A., 2021. Free transverse vibration analysis of laminated composite beams with arbitrary number of concentrated masses. *Archive of Applied Mechanics*, *91*(6), pp.2393-2402.

[46] Vlasov VZ., 1961. Thin Walled Elastic Beams. Jerusalem: Israel Program for Scientific.

[47] Lee, J., Kim, S.E. and Hong, K., 2002. Lateral buckling of I-section composite beams. *Engineering Structures*, *24*(7), pp.955-964.

[48] Raftoyiannis, I.G. and Adamakos, T., 2010. Critical lateral-torsional buckling moments of steel web-tapered I-beams. *The Open Construction and Building Technology Journal*, *4*(1).

[49] Osmani, A. and Meftah, S.A., 2018. Lateral buckling of tapered thin walled bi-symmetric beams under combined axial and bending loads with shear deformations allowed. *Engineering Structures*, *165*, pp.76-87.

[50] ANSYS, Version 5.4, Swanson Analysis System, Inc, 2007.